Search for high-mass resonances decaying into ZZ in $p\bar{p}$ collisions at $\sqrt{s} = 1.96$ TeV

T. Aaltonen,[21] B. Álvarez González,[9,aa] S. Amerio,[40a] D. Amidei,[32] A. Anastassov,[15,y] A. Annovi,[17] J. Antos,[12] G. Apollinari,[15] J. A. Appel,[15] T. Arisawa,[54] A. Artikov,[13] J. Asaadi,[49] W. Ashmanskas,[15] B. Auerbach,[57] A. Aurisano,[49] F. Azfar,[39] W. Badgett,[15] T. Bae,[25] A. Barbaro-Galtieri,[26] V. E. Barnes,[44] B. A. Barnett,[23] P. Barria,[42a,42c] P. Bartos,[12] M. Bauce,[40a,40b] F. Bedeschi,[42a] S. Behari,[23] G. Bellettini,[42a,42b] J. Bellinger,[56] D. Benjamin,[14] A. Beretvas,[15] A. Bhatti,[46] D. Bisello,[40a,40b] I. Bizjak,[28] K. R. Bland,[5] B. Blumenfeld,[23] A. Bocci,[14] A. Bodek,[45] D. Bortoletto,[44] J. Boudreau,[43] A. Boveia,[11] L. Brigliadori,[6a,6b] C. Bromberg,[33] E. Brucken,[21] J. Budagov,[13] H. S. Budd,[45] K. Burkett,[15] G. Busetto,[40a,40b] P. Bussey,[19] A. Buzatu,[31] A. Calamba,[10] C. Calancha,[29] S. Camarda,[4] M. Campanelli,[28] M. Campbell,[32] F. Canelli,[11,15] B. Carls,[22] D. Carlsmith,[56] R. Carosi,[42a] S. Carrillo,[16,n] S. Carron,[15] B. Casal,[9,l] M. Casarsa,[50a] A. Castro,[6a,6b] P. Catastini,[20] D. Cauz,[50a] V. Cavaliere,[22] M. Cavalli-Sforza,[4] A. Cerri,[26,g] L. Cerrito,[28,t] Y. C. Chen,[1] M. Chertok,[7] G. Chiarelli,[42a] G. Chlachidze,[15] F. Chlebana,[15] K. Cho,[25] D. Chokheli,[13] W. H. Chung,[56] Y. S. Chung,[45] M. A. Ciocci,[42a,42c] A. Clark,[18] C. Clarke,[55] G. Compostella,[40a,40b] M. E. Convery,[15] J. Conway,[7] M. Corbo,[15] M. Cordelli,[17] C. A. Cox,[7] D. J. Cox,[7] F. Crescioli,[42a,42b] J. Cuevas,[9,aa] R. Culbertson,[15] D. Dagenhart,[15] N. d'Ascenzo,[15,x] M. Datta,[15] P. de Barbaro,[45] M. Dell'Orso,[42a,42b] L. Demortier,[46] M. Deninno,[6a] F. Devoto,[21] M. d'Errico,[40a,40b] A. Di Canto,[42a,42b] B. Di Ruzza,[15] J. R. Dittmann,[5] M. D'Onofrio,[27] S. Donati,[42a,42b] P. Dong,[15] M. Dorigo,[50a] T. Dorigo,[40a] K. Ebina,[54] A. Elagin,[49] A. Eppig,[32] R. Erbacher,[7] S. Errede,[22] N. Ershaidat,[15,ee] R. Eusebi,[49] S. Farrington,[39] M. Feindt,[24] J. P. Fernandez,[29] R. Field,[16] G. Flanagan,[15,v] R. Forrest,[7] M. J. Frank,[5] M. Franklin,[20] J. C. Freeman,[15] Y. Funakoshi,[54] I. Furic,[16] M. Gallinaro,[46] J. E. Garcia,[18] A. F. Garfinkel,[44] P. Garosi,[42a,42c] H. Gerberich,[22] E. Gerchtein,[15] S. Giagu,[47a] V. Giakoumopoulou,[3] P. Giannetti,[42a] K. Gibson,[43] C. M. Ginsburg,[15] N. Giokaris,[3] P. Giromini,[17] G. Giurgiu,[23] V. Glagolev,[13] D. Glenzinski,[15] M. Gold,[35] D. Goldin,[49] N. Goldschmidt,[16] A. Golossanov,[15] G. Gomez,[9] G. Gomez-Ceballos,[30] M. Goncharov,[30] O. González,[29] I. Gorelov,[35] A. T. Goshaw,[14] K. Goulianos,[46] S. Grinstein,[4] C. Grosso-Pilcher,[11] R. C. Group,[53,15] J. Guimaraes da Costa,[20] S. R. Hahn,[15] E. Halkiadakis,[48] A. Hamaguchi,[38] J. Y. Han,[45] F. Happacher,[17] K. Hara,[51] D. Hare,[48] M. Hare,[52] R. F. Harr,[55] K. Hatakeyama,[5] C. Hays,[39] M. Heck,[24] J. Heinrich,[41] M. Herndon,[56] S. Hewamanage,[5] A. Hocker,[15] W. Hopkins,[15,h] D. Horn,[24] S. Hou,[1] R. E. Hughes,[36] M. Hurwitz,[11] U. Husemann,[57] N. Hussain,[31] M. Hussein,[33] J. Huston,[33] G. Introzzi,[42a] M. Iori,[47a,47b] A. Ivanov,[7,q] E. James,[15] D. Jang,[10] B. Jayatilaka,[14] E. J. Jeon,[25] S. Jindariani,[15] M. Jones,[44] K. K. Joo,[25] S. Y. Jun,[10] T. R. Junk,[15] T. Kamon,[25,49] P. E. Karchin,[55] A. Kasmi,[5] Y. Kato,[38,p] W. Ketchum,[11] J. Keung,[41] V. Khotilovich,[49] B. Kilminster,[15] D. H. Kim,[25] H. S. Kim,[25] J. E. Kim,[25] M. J. Kim,[17] S. B. Kim,[25] S. H. Kim,[51] Y. K. Kim,[11] Y. J. Kim,[25] N. Kimura,[54] M. Kirby,[15] S. Klimenko,[16] K. Knoepfel,[15] K. Kondo,[54,a] D. J. Kong,[25] J. Konigsberg,[16] A. V. Kotwal,[14] M. Kreps,[24] J. Kroll,[41] D. Krop,[11] M. Kruse,[14] V. Krutelyov,[49,d] T. Kuhr,[24] M. Kurata,[51] S. Kwang,[11] A. T. Laasanen,[44] S. Lami,[42a] S. Lammel,[15] M. Lancaster,[28] R. L. Lander,[7] K. Lannon,[36,z] A. Lath,[48] G. Latino,[42a,42c] T. LeCompte,[2] E. Lee,[49] H. S. Lee,[11,r] J. S. Lee,[25] S. W. Lee,[49,cc] S. Leo,[42a,42b] S. Leone,[42a] J. D. Lewis,[15] A. Limosani,[14,u] C.-J. Lin,[26] M. Lindgren,[15] E. Lipeles,[41] A. Lister,[18] D. O. Litvintsev,[15] C. Liu,[43] H. Liu,[53] Q. Liu,[44] T. Liu,[15] S. Lockwitz,[57] A. Loginov,[57] D. Lucchesi,[40a,40b] J. Lueck,[24] P. Lujan,[26] P. Lukens,[15] G. Lungu,[46] J. Lys,[26] R. Lysak,[12,f] R. Madrak,[15] K. Maeshima,[15] P. Maestro,[42a,42c] S. Malik,[46] G. Manca,[27,b] A. Manousakis-Katsikakis,[3] F. Margaroli,[47a] C. Marino,[24] M. Martínez,[4] P. Mastrandrea,[47a] K. Matera,[22] M. E. Mattson,[55] A. Mazzacane,[15] P. Mazzanti,[6a] K. S. McFarland,[45] P. McIntyre,[49] R. McNulty,[27,k] A. Mehta,[27] P. Mehtala,[21] C. Mesropian,[46] T. Miao,[15] D. Mietlicki,[32] A. Mitra,[1] H. Miyake,[51] S. Moed,[15] N. Moggi,[6a] M. N. Mondragon,[15,n] C. S. Moon,[25] R. Moore,[15] M. J. Morello,[42a,42d] J. Morlock,[24] P. Movilla Fernandez,[15] A. Mukherjee,[15] Th. Muller,[24] P. Murat,[15] M. Mussini,[6a,6b] J. Nachtman,[15,o] Y. Nagai,[51] J. Naganoma,[54] I. Nakano,[37] A. Napier,[52] J. Nett,[49] C. Neu,[53] M. S. Neubauer,[22] J. Nielsen,[26,e] L. Nodulman,[2] S. Y. Noh,[25] O. Norniella,[22] L. Oakes,[39] S. H. Oh,[14] Y. D. Oh,[25] I. Oksuzian,[53] T. Okusawa,[38] R. Orava,[21] L. Ortolan,[4] S. Pagan Griso,[40a,40b] C. Pagliarone,[50a] E. Palencia,[9,g] V. Papadimitriou,[15] A. A. Paramonov,[2] J. Patrick,[15] G. Pauletta,[50a,50b] M. Paulini,[10] C. Paus,[30] D. E. Pellett,[7] A. Penzo,[50a] T. J. Phillips,[14] G. Piacentino,[42a] E. Pianori,[41] J. Pilot,[36] K. Pitts,[22] C. Plager,[8] L. Pondrom,[56] S. Poprocki,[15,h] K. Potamianos,[44] F. Prokoshin,[13,dd] A. Pranko,[26] F. Ptohos,[17,i] G. Punzi,[42a,42b] A. Rahaman,[43] V. Ramakrishnan,[56] N. Ranjan,[44] I. Redondo,[29] P. Renton,[39] M. Rescigno,[47a] T. Riddick,[28] F. Rimondi,[6a,6b] L. Ristori,[42a,15] A. Robson,[19] T. Rodrigo,[9] T. Rodriguez,[41] E. Rogers,[22] S. Rolli,[52,j] R. Roser,[15] F. Ruffini,[42a,42c] A. Ruiz,[9] J. Russ,[10] V. Rusu,[15] A. Safonov,[49] W. K. Sakumoto,[45] Y. Sakurai,[54] L. Santi,[50a,50b] K. Sato,[51] V. Saveliev,[15,x] A. Savoy-Navarro,[15,bb] P. Schlabach,[15] A. Schmidt,[24] E. E. Schmidt,[15] T. Schwarz,[15] L. Scodellaro,[9] A. Scribano,[42a,42c] F. Scuri,[42a] S. Seidel,[35] Y. Seiya,[38] A. Semenov,[13] F. Sforza,[42a,42c] S. Z. Shalhout,[7] T. Shears,[27] P. F. Shepard,[43] M. Shimojima,[51,w] M. Shochet,[11] I. Shreyber-Tecker,[34] A. Simonenko,[13] P. Sinervo,[31]

K. Sliwa,[52] J. R. Smith,[7] F. D. Snider,[15] A. Soha,[15] V. Sorin,[4] H. Song,[43] P. Squillacioti,[42a,42c] M. Stancari,[15] R. St. Denis,[19] B. Stelzer,[31] O. Stelzer-Chilton,[31] D. Stentz,[15,y] J. Strologas,[35] G. L. Strycker,[32] Y. Sudo,[51] A. Sukhanov,[15] I. Suslov,[13] K. Takemasa,[51] Y. Takeuchi,[51] J. Tang,[11] M. Tecchio,[32] P. K. Teng,[1] J. Thom,[15,h] J. Thome,[10] G. A. Thompson,[22] E. Thomson,[41] D. Toback,[49] S. Tokar,[12] K. Tollefson,[33] T. Tomura,[51] D. Tonelli,[15] S. Torre,[17] D. Torretta,[15] P. Totaro,[40a] M. Trovato,[42a,42d] F. Ukegawa,[51] S. Uozumi,[25] A. Varganov,[32] F. Vázquez,[16,n] G. Velev,[15] C. Vellidis,[15] M. Vidal,[44] I. Vila,[9] R. Vilar,[9] J. Vizán,[9] M. Vogel,[35] G. Volpi,[17] P. Wagner,[41] R. L. Wagner,[15] T. Wakisaka,[38] R. Wallny,[8] S. M. Wang,[1] A. Warburton,[31] D. Waters,[28] W. C. Wester III,[15] D. Whiteson,[41,c] A. B. Wicklund,[2] E. Wicklund,[15] S. Wilbur,[11] F. Wick,[24] H. H. Williams,[41] J. S. Wilson,[36] P. Wilson,[15] B. L. Winer,[36] P. Wittich,[15,h] S. Wolbers,[15] H. Wolfe,[36] T. Wright,[32] X. Wu,[18] Z. Wu,[5] K. Yamamoto,[38] D. Yamato,[38] T. Yang,[15] U. K. Yang,[11,s] Y. C. Yang,[25] W.-M. Yao,[26] G. P. Yeh,[15] K. Yi,[15,o] J. Yoh,[15] K. Yorita,[54] T. Yoshida,[38,m] G. B. Yu,[14] I. Yu,[25] S. S. Yu,[15] J. C. Yun,[15] A. Zanetti,[50a] Y. Zeng,[14] C. Zhou,[14] and S. Zucchelli[6a,6b]

(CDF Collaboration)

[1]*Institute of Physics, Academia Sinica, Taipei, Taiwan 11529, Republic of China*
[2]*Argonne National Laboratory, Argonne, Illinois 60439, USA*
[3]*University of Athens, 157 71 Athens, Greece*
[4]*Institut de Fisica d'Altes Energies, ICREA, Universitat Autonoma de Barcelona, E-08193, Bellaterra (Barcelona), Spain*
[5]*Baylor University, Waco, Texas 76798, USA*
[6a]*Istituto Nazionale di Fisica Nucleare Bologna, I-40127 Bologna, Italy*
[6b]*University of Bologna, I-40127 Bologna, Italy*
[7]*University of California, Davis, Davis, California 95616, USA*
[8]*University of California, Los Angeles, Los Angeles, California 90024, USA*
[9]*Instituto de Fisica de Cantabria, CSIC-University of Cantabria, 39005 Santander, Spain*
[10]*Carnegie Mellon University, Pittsburgh, Pennsylvania 15213, USA*
[11]*Enrico Fermi Institute, University of Chicago, Chicago, Illinois 60637, USA*
[12]*Comenius University, 842 48 Bratislava, Slovakia; Institute of Experimental Physics, 040 01 Kosice, Slovakia*
[13]*Joint Institute for Nuclear Research, RU-141980 Dubna, Russia*
[14]*Duke University, Durham, North Carolina 27708, USA*
[15]*Fermi National Accelerator Laboratory, Batavia, Illinois 60510, USA*
[16]*University of Florida, Gainesville, Florida 32611, USA*
[17]*Laboratori Nazionali di Frascati, Istituto Nazionale di Fisica Nucleare, I-00044 Frascati, Italy*
[18]*University of Geneva, CH-1211 Geneva 4, Switzerland*
[19]*Glasgow University, Glasgow G12 8QQ, United Kingdom*
[20]*Harvard University, Cambridge, Massachusetts 02138, USA*
[21]*Division of High Energy Physics, Department of Physics, University of Helsinki and Helsinki Institute of Physics, FIN-00014, Helsinki, Finland*
[22]*University of Illinois, Urbana, Illinois 61801, USA*
[23]*The Johns Hopkins University, Baltimore, Maryland 21218, USA*
[24]*Institut für Experimentelle Kernphysik, Karlsruhe Institute of Technology, D-76131 Karlsruhe, Germany*
[25]*Center for High Energy Physics: Kyungpook National University, Daegu 702-701, Korea; Seoul National University, Seoul 151-742, Korea; Sungkyunkwan University, Suwon 440-746, Korea; Korea Institute of Science and Technology Information, Daejeon 305-806, Korea; Chonnam National University, Gwangju 500-757, Korea; Chonbuk National University, Jeonju 561-756, Korea*
[26]*Ernest Orlando Lawrence Berkeley National Laboratory, Berkeley, California 94720, USA*
[27]*University of Liverpool, Liverpool L69 7ZE, United Kingdom*
[28]*University College London, London WC1E 6BT, United Kingdom*
[29]*Centro de Investigaciones Energeticas Medioambientales y Tecnologicas, E-28040 Madrid, Spain*
[30]*Massachusetts Institute of Technology, Cambridge, Massachusetts 02139, USA*
[31]*Institute of Particle Physics: McGill University, Montréal, Québec, Canada H3A 2T8; Simon Fraser University, Burnaby, British Columbia, Canada V5A 1S6; University of Toronto, Toronto, Ontario, Canada M5S 1A7; and TRIUMF, Vancouver, British Columbia, Canada V6T 2A3*
[32]*University of Michigan, Ann Arbor, Michigan 48109, USA*
[33]*Michigan State University, East Lansing, Michigan 48824, USA*
[34]*Institution for Theoretical and Experimental Physics, ITEP, Moscow 117259, Russia*

[35]University of New Mexico, Albuquerque, New Mexico 87131, USA
[36]The Ohio State University, Columbus, Ohio 43210, USA
[37]Okayama University, Okayama 700-8530, Japan
[38]Osaka City University, Osaka 588, Japan
[39]University of Oxford, Oxford OX1 3RH, United Kingdom
[40a]Istituto Nazionale di Fisica Nucleare, Sezione di Padova-Trento, I-35131 Padova, Italy
[40b]University of Padova, I-35131 Padova, Italy
[41]University of Pennsylvania, Philadelphia, Pennsylvania 19104, USA
[42a]Istituto Nazionale di Fisica Nucleare Pisa, I-56127 Pisa, Italy
[42b]University of Pisa, I-56127 Pisa, Italy
[42c]University of Siena, I-56127 Pisa, Italy
[42d]Scuola Normale Superiore, I-56127 Pisa, Italy
[43]University of Pittsburgh, Pittsburgh, Pennsylvania 15260, USA
[44]Purdue University, West Lafayette, Indiana 47907, USA
[45]University of Rochester, Rochester, New York 14627, USA
[46]The Rockefeller University, New York, New York 10065, USA
[47a]Istituto Nazionale di Fisica Nucleare, Sezione di Roma 1, I-00185 Roma, Italy
[47b]Sapienza Università di Roma, I-00185 Roma, Italy
[48]Rutgers University, Piscataway, New Jersey 08855, USA
[49]Texas A&M University, College Station, Texas 77843, USA
[50a]Istituto Nazionale di Fisica Nucleare Trieste/Udine, I-34100 Trieste, Italy
[50b]University of Udine, I-33100 Udine, Italy
[51]University of Tsukuba, Tsukuba, Ibaraki 305, Japan
[52]Tufts University, Medford, Massachusetts 02155, USA
[53]University of Virginia, Charlottesville, Virginia 22906, USA
[54]Waseda University, Tokyo 169, Japan
[55]Wayne State University, Detroit, Michigan 48201, USA
[56]University of Wisconsin, Madison, Wisconsin 53706, USA
[57]Yale University, New Haven, Connecticut 06520, USA
(Received 15 November 2011; published 24 January 2012)

We search for high-mass resonances decaying into Z boson pairs using data corresponding to 6 fb^{-1} collected by the CDF experiment in $p\bar{p}$ collisions at $\sqrt{s} = 1.96$ TeV. The search is performed in three distinct final states: $ZZ \to \ell^+\ell^-\ell^+\ell^-$, $ZZ \to \ell^+\ell^-\nu\nu$, and $ZZ \to \ell^+\ell^- jj$. For a Randall-Sundrum graviton G^*, the 95% CL upper limits on the production cross section times branching ratio to ZZ, $\sigma(p\bar{p} \to G^* \to ZZ)$, vary between 0.26 pb and 0.045 pb in the mass range $300 < M_{G^*} < 1000$ GeV$/c^2$.

DOI: 10.1103/PhysRevD.85.012008 PACS numbers: 13.85.Rm, 14.70.Hp, 14.70.Kv

I. INTRODUCTION

We report the results of a search for high-mass resonances decaying to ZZ in $p\bar{p}$ collisions at $\sqrt{s} = 1.96$ TeV at the Tevatron. Although the decay of the standard model Higgs boson to ZZ is expected to be beyond the sensitivity of the Tevatron experiments [1], new physics could affect ZZ production in different ways. In models containing large extra dimensions the ZZ production cross section is increased through loop corrections [2]. Resonances appearing at high mass such as a Randall-Sundrum (RS) graviton [3] could decay manifestly to two Z bosons. The original RS model predicts Kaluza-Klein excitations of the graviton (G^*) that decay predominantly to a pair of charged leptons or a pair of photons. Experimental searches for such high-mass resonance decays have excluded RS graviton states up to a mass of around 1 TeV$/c^2$ at 95% confidence level for a natural choice of coupling parameter [4], both at the Tevatron and at the LHC [5]. However, in RS models that have standard model fields propagating in the bulk, the G^* couplings to light fermions and photons may be heavily suppressed so that the dominant decay modes are to $t\bar{t}$, Higgs pairs, or pairs of heavy bosons [6]. Furthermore, in some models the decay to heavy bosons is dominant [7]. Suppression of the couplings to light fermions also results in gluon fusion becoming the primary production process.

The CDF experiment has previously searched for resonances decaying to Z pairs and excluded RS gravitons with mass up to around 0.5 TeV$/c^2$ at 95% confidence level [8]. The search described in this paper gives improved sensitivity over the previous analysis through modified event selection, the inclusion of extra final states, and the addition of more data. Three final states are examined, corresponding to the different Z boson decay modes $ZZ \to \ell^+\ell^-\ell^+\ell^-$, $ZZ \to \ell^+\ell^-\nu\nu$, and $ZZ \to \ell^+\ell^- jj$, where ℓ is an electron or muon and j is a hadronic jet. These three channels have different signal-to-background

ratios and allow an overconstrained search. The four-lepton final state has the smallest background; however, depending on the resonance mass, the best single-channel sensitivity is provided by either the $ZZ \to \ell^+\ell^- jj$ or $ZZ \to \ell^+\ell^-\nu\nu$ channels.

The paper is organized as follows: in Sec. II we introduce the CDF detector and trigger system; in Sec. III we describe the reconstruction and identification procedures; then in Secs. VI, VII, and VIII we report the search results from each of the channels $ZZ \to \ell^+\ell^-\ell^+\ell^-$, $ZZ \to \ell^+\ell^-\nu\nu$ and $ZZ \to \ell^+\ell^- jj$. Section VII gives limits resulting from all three channels and their combination.

II. DETECTOR

The CDF II detector is a general-purpose particle detector, described in detail elsewhere [9]. The results reported in this paper use information from several detector subsystems for charged lepton and jet reconstruction and identification.

Tracks of charged particles are reconstructed in the silicon system [10] and in the central tracker [11], which is a drift chamber that consists of 96 layers of sense wires grouped into eight ''superlayers''. Superlayers alternate between an axial configuration, with sense wires parallel to the colliding beams, and a small-angle stereo configuration. For high momentum tracks the resolution is $\sigma_{p_T}/p_T^2 \simeq 1.7 \times 10^{-3}\ (\mathrm{GeV}/c)^{-1}$, where $p_T = p\sin\theta$, p being the track momentum and θ the polar angle with respect to the proton beam direction.

The calorimeter is segmented radially into electromagnetic and hadronic compartments [12,13]. The central calorimeter is split at the center into two separate barrels and covers the pseudorapidity range $|\eta| < 1.1$ (where $\eta = -\ln\tan\frac{\theta}{2}$). Each barrel consists of 24 azimuthal wedges segmented in projective towers of 0.1 in η. The forward calorimeter segmentation increases from 0.1 in η and 7.5° in the azimuthal angle ϕ at $\eta = 1.1$, to 0.5 in η and 15° in ϕ at $\eta = 3.6$. Electron energy resolutions are $13.5\%/\sqrt{E_T} \oplus 2\%$ in the central calorimeter and $16\%/\sqrt{E} \oplus 1\%$ in the forward calorimeters, where $E_T = E\sin\theta$. The electromagnetic calorimeters incorporate shower maximum detectors that are used to measure shower profiles with spatial resolution of around 2 mm.

Dedicated muon detectors [14] are mounted around the calorimeters, providing coverage for $|\eta| \lesssim 1.5$. Luminosity is measured by a hodoscopic system of Cherenkov counters [15].

CDF has a three-level online trigger system. The data used in this measurement were collected using inclusive high-p_T electron and muon triggers, and a two-electron trigger. The single-lepton triggers select events that have electron or muon candidates with $p_T \geq 18\ \mathrm{GeV}/c$ and $|\eta| \lesssim 1.0$ [16], and the two-electron trigger uses only calorimeter information and allows electron candidates above the same p_T threshold anywhere in the detector. The data correspond to an integrated luminosity of 6 fb^{-1} collected between February 2002 and February 2010.

III. RECONSTRUCTION AND IDENTIFICATION

In this section we discuss lepton reconstruction and identification, and reconstruction of jets and missing transverse energy.

A. Leptons

Decays of a heavy resonance to ZZ, where at least one of the Z bosons decays leptonically, result in a wide lepton energy spectrum. Any inefficiency in lepton reconstruction and identification is raised to the fourth power in the $ZZ \to \ell^+\ell^-\ell^+\ell^-$ channel. Thus, keeping efficiency high while maintaining stringent background rejection is equally important for $p_T \sim 20\ \mathrm{GeV}/c$ and for $p_T > 100\ \mathrm{GeV}/c$. To this end, this analysis incorporates several refinements in the offline reconstruction and identification of electron and muon candidates. Studies were performed on inclusive $Z \to \ell^+\ell^-$ candidates and on events containing one lepton plus two additional tracks having $p_T > 10\ \mathrm{GeV}/c$, and this latter data set was fully reprocessed for the $ZZ \to \ell^+\ell^-\ell^+\ell^-$ analysis.

First we describe the elements of the lepton selection that are standard to CDF. Electron candidates consist of a calorimeter cluster matched to a well-reconstructed track. Candidates are required to be within the fiducial region of the shower maximum detectors and have a shower that is mostly contained in the electromagnetic compartment of the calorimeter, with a shower shape that is consistent with test beam expectation [17]. For candidates reconstructed in the central part of the detector ($|\eta| < 1.1$), the matched track must have $p_T > 10\ \mathrm{GeV}/c$, pass through all layers of the central tracker, and have a fit $\chi^2/\mathrm{d.o.f.} < 3$. Candidates reconstructed in the forward part of the detector, $1.13 < |\eta| < 2.8$, must either have a track in the central tracker, or a track in the silicon system with ≥ 5 hits.

A muon candidate is reconstructed from a track in the central tracker pointing to track segments in the muon chambers. Muon track trajectories must be such that at least 30 central tracker hits would be expected geometrically, and at least 60% of those must be found. Tracks pointing forward ($|\eta| \gtrsim 1$) that have fewer than three central tracker segments in axial superlayers must also have at least five $r-\phi$ hits in the silicon tracking system. Muon energy deposition in the calorimeter must be consistent with that of a minimally-ionizing particle. We also consider minimally-ionizing tracks that have no track segments in the muon systems as muon candidates.

Electron and muon candidates are required to have $E_T > 15$ GeV and $p_T > 15\ \mathrm{GeV}/c$ respectively. In addition, one of the lepton candidates in each event is required to have $E_T > 20$ GeV (electrons) or $p_T > 20\ \mathrm{GeV}/c$ (muons), and to pass more restrictive quality requirements. These extra requirements are that the lepton track must have at least

three segments reconstructed in the axial superlayers and three in the stereo superlayers; and the track of a muon candidate must also be well-matched to a track segment reconstructed in the muon system.

The first refinement in lepton selection is in the isolation requirement made on all lepton candidates. The "isolation energy" is the amount of energy reconstructed in a cone of $\Delta R < 0.4$ around a lepton candidate, where $\Delta R = \sqrt{(\Delta\eta)^2 + (\Delta\phi)^2}$. In computing the isolation energy, we refine the treatment of energy leakage across calorimeter cell boundaries. In the central calorimeter, electron clusters include energy depositions from only a single wedge in ϕ. As each calorimeter tower is read out from different ϕ sides by two photomultiplier tubes, the relative heights of the pulses locate the energy deposition in ϕ. Locating the center of the energy depositions in towers neighboring the electron cluster allows us to estimate the leakage, and correct the isolation energy variable event-by-event, rather than by applying an average correction. The correction method is validated by examining the isolation energy as a function of shower position in the calorimeter cell, which is found to be more uniform than under application of the standard average correction, as shown in Fig. 1(a). Muons are not expected to result in energy leakage; their isolation energy is also shown in Fig. 1(a) as validation of the method. The average isolation energy should depend on the instantaneous luminosity but not on the lepton E_T, and its uniformity in lepton E_T is confirmed by Fig. 1(b). All electron and muon candidates are therefore required to be isolated in the calorimeter by limiting the isolation energy to be below 4 GeV. Cutting on isolation energy, rather than requiring the standard ratio of isolation energy to lepton momentum to be <0.1 [17], increases the acceptance for $ZZ \to \ell^+\ell^-\ell^+\ell^-$ events by 4%.

For the $ZZ \to \ell^+\ell^-\ell^+\ell^-$ analysis, events have been reconstructed with an updated version of the CDF tracking code that gives improved pattern recognition at high luminosities. The updated version includes an extra algorithm to associate hits in the central tracker with silicon-only tracks from electron candidates in the forward region of the detector. Adding extra hits on to these tracks improves the robustness of forward electron charge identification.

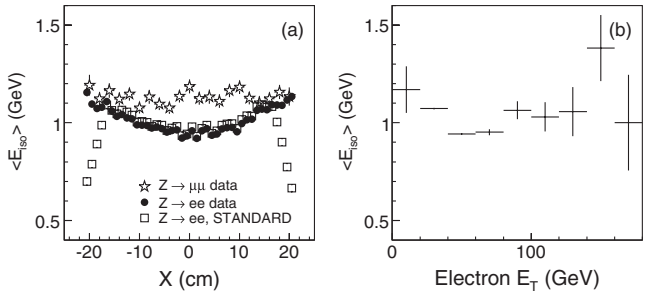

FIG. 1. (a) Corrected isolation energy across the calorimeter wedge coordinate X in $Z \to e^+e^-$ (new correction: solid circles; standard correction: open squares) and $Z \to \mu^+\mu^-$ (new correction: open stars) events; (b) average calorimeter isolation energy as a function of electron E_T in $Z \to e^+e^-$ events.

Use of an improved reconstruction algorithm in the central shower maximum detector gives better separation between showers generated by electron tracks and showers produced by bremsstrahlung photons. Matching tracks to the showers they initiate in both coordinate and energy improves hadron rejection and allows the inclusion of electron candidates that lose a significant amount of energy through bremsstrahlung. The improved background rejection allows the relaxation of other standard electron identification requirements and, overall, the selection efficiency is increased by around 9% per electron.

Electrons reconstructed in the edge ϕ-rings of the calorimeter on either side of the gap between the central and forward detectors are generally excluded from analysis. They are included here, after verification that they have energy resolution comparable with electrons reconstructed in the bulk of the detectors, and are well-modeled in the simulation. This increases electron acceptance by around 10% per electron.

The combined effect of the refinements described above is to increase lepton acceptance without increasing fake lepton backgrounds, as measured by jet-to-lepton fake rates in inclusive jet datasets. The lepton selection used for this analysis is validated by measuring inclusive $Z \to \ell^+\ell^-$ cross-sections and separating events by calorimeter region and muon system. We verify that for each subset of events the measurement is stable in time, and combining all channels we measure $\sigma(p\bar{p} \to Z) \times Br(Z \to \ell^+\ell^-) = 247 \pm 6(\text{stat} + \text{syst}) \pm 15(\text{lumi})$ pb, consistent with CDF's measurement [16].

B. Jets and $\not\!\!E_T$

Jets are reconstructed as clustered energy depositions in the calorimeter using a fixed cone clustering algorithm with cone size $\Delta R = 0.4$ [18]. Jet energies are corrected for η-dependent calorimeter response and for multiple interactions [19]. We consider jets having $E_T > 20$ GeV.

The missing transverse energy ($\not\!\!E_T$) is defined as the sum over calorimeter tower energies $\vec{\not\!\!E}_T = -\sum_i E_T^i \mathbf{n_i}$, where $\mathbf{n_i}$ is the unit vector in the transverse plane that points to calorimeter tower i. The $\not\!\!E_T$ is adjusted to account for the energy corrections made to reconstructed jets, and for muons identified in the event. As neutrinos pass through the detector without depositing energy, large $\not\!\!E_T$ in an event can imply the presence of high-energy neutrinos.

IV. $ZZ \to \ell^+\ell^-\ell^+\ell^-$ CHANNEL

The first search channel is $ZZ \to \ell^+\ell^-\ell^+\ell^-$. We select events with four candidate charged leptons, which may be electrons or muons. At least two of the four must have $E_T > 20$ GeV for electron candidates ($p_T > 20$ GeV/c for

muon candidates) and pass the more restrictive lepton selection; and in order to have the trigger efficiency well-defined, at least one must satisfy the trigger requirements.

Leptons of the same flavor are paired to form Z candidates, seeded by a lepton that passes the tighter selection. In the case of four-electron or four-muon candidates, the pairings that minimize the χ^2 of the ZZ hypothesis are chosen:

$$\chi^2 = (M_{12} - M_Z)^2/\sigma_M^2 + (M_{34} - M_Z)^2/\sigma_M^2,$$

where M_{12} and M_{34} are the masses of the lepton pairs, $\sigma_M = 3$ GeV$/c^2$ approximates experimental resolution in $M_{\ell\ell}$ for both electron and muon decays, and M_Z is the mass of the Z boson.

We find ten events that pass the four-lepton selection. In all of these events the number of leptons of the same flavor is even. The best pairings of the ten candidate events are all oppositely-charged. To minimize the effect of Z/γ^* interference, both Z boson candidates are required to be within 15 GeV$/c^2$ of the Z pole, $76 < M_{\ell\ell} < 106$ GeV$/c^2$. Following this requirement, eight event candidates remain: two events have four reconstructed electrons ($eeee$), three have two electrons and two muons ($ee\mu\mu$), and the remaining three have four reconstructed muons ($\mu\mu\mu\mu$). The two events that fail the Z mass requirement both have one Z candidate with invariant mass below 60 GeV$/c^2$.

We use the selected events to measure the $p\bar{p} \to ZZ$ production cross section. On- and off-shell ZZ production, as shown in Fig. 2, followed by Z boson decays to charged leptons, is the only lowest-order standard model process that results in a final state with four high-p_T leptons produced in the primary interaction. The background in this channel thus comes only from misidentification. The main contributions are: $p\bar{p} \to WZ$ + jet with a jet misidentified as a lepton; $p\bar{p} \to Z$ + 2 jets with both jets misidentified as leptons; and $p\bar{p} \to Z + \gamma$ + jet with both the photon and the jet misidentified as electrons. The contribution from $t\bar{t}$ production is an order of magnitude smaller than that of WZ production. As a result of the $M_{\ell\ell} > 76$ GeV$/c^2$ requirement, the contribution of $Z \to \tau\tau$ decays is negligible.

The PYTHIA event generator [20] and the full CDF detector simulation [21] are used to simulate kinematics of these processes and photon-to-lepton misidentification. Jet-to-lepton misidentification rates are measured in inclusive jet data and found to be of the order of 10^{-4}–10^{-3} per jet for $15 < E_T < 100$ GeV. These misidentification rates are used to weight the simulated events of the background processes, resulting in a total background yield estimated to be less than 0.01 event.

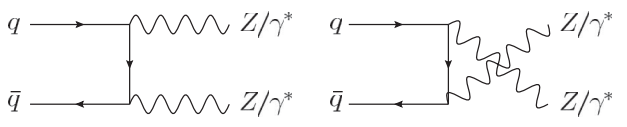

FIG. 2. Lowest-order standard model ZZ production.

The acceptance for standard model $p\bar{p} \to Z/\gamma^* Z/\gamma^* \to \ell^+\ell^-\ell^+\ell^-$ is determined using the leading-order PYTHIA generator and found to be 0.17 ± 0.02. The uncertainty has contributions from higher-order generator effects, lepton identification, and trigger efficiency uncertainty. In order to estimate the uncertainty arising from higher-order generator effects, the MC@NLO generator [22] is used, interfaced to HERWIG [23] to provide parton showering and hadronization. The corresponding relative uncertainty on the acceptance is estimated to be 2.7%. Lepton identification efficiencies are measured in the data using candidate $Z \to \ell^+\ell^-$ events with uncertainties at the level of 1%. We also account for a small drop in lepton identification efficiency with time and assign a 2% relative uncertainty per lepton for residual run-dependent effects. We assume no correlation between the uncertainties on electron and muon reconstruction, and full correlation between the uncertainties for leptons of the same flavor. The trigger efficiency per four-lepton event is close to unity, with a systematic uncertainty of less than 0.5%.

Given the branching fraction for $Z \to \ell^+\ell^- = (3.366 \pm 0.002)\%$ [24], the branching fraction for two Z bosons to decay to electrons or muons is 4.52×10^{-3}. The scale factor to take into account differences in triggering, reconstruction and identification efficiencies between data and simulation is 0.80 ± 0.08, and the integrated luminosity is 5.91 ± 0.35 fb^{-1}. Experimentally, we observe $p\bar{p} \to Z/\gamma^* Z/\gamma^* \to \ell^+\ell^-\ell^+\ell^-$, and to compare our measurement with the theoretical prediction of $p\bar{p} \to ZZ$, calculated in a narrow pole approximation [25], we account for Z/γ^* interference. The interference in the region $76 < M_{\ell\ell} < 106$ GeV$/c^2$ increases the acceptance by a factor of 1.03. From simulation, the fraction of ZZ events that falls outside the region $76 < M_{\ell\ell} < 106$ GeV$/c^2$ is 0.07 and is also corrected for. The eight observed events therefore result in a cross section:

$$\sigma(p\bar{p} \to ZZ) = 2.3^{+0.9}_{-0.8}(\text{stat.}) \pm 0.2(\text{syst.}) \text{ pb}$$

where the statistical uncertainty is the 68% confidence interval given by the method of Feldman and Cousins [26]. The value is consistent with the theoretical prediction 1.4 ± 0.1 pb [25]. A more precise measurement of the ZZ cross section, which combines four-lepton and leptons plus $\not\!\!E_T$ channels, is reported elsewhere [27].

Examining the properties of the eight ZZ candidate events we find an excess of events over standard model expectations at high invariant mass, M_{ZZ}. The invariant masses of four events are clustered with mean 327 GeV$/c^2$, as shown in Fig. 3. All four candidates, one $eeee$, one $ee\mu\mu$, and two $\mu\mu\mu\mu$, have values of M_{ZZ} within 7 GeV$/c^2$ of the mean. In the four-lepton channel the detector resolution in M_{ZZ}, $\sigma(M_{ZZ})$, is 5 to 6 GeV$/c^2$,

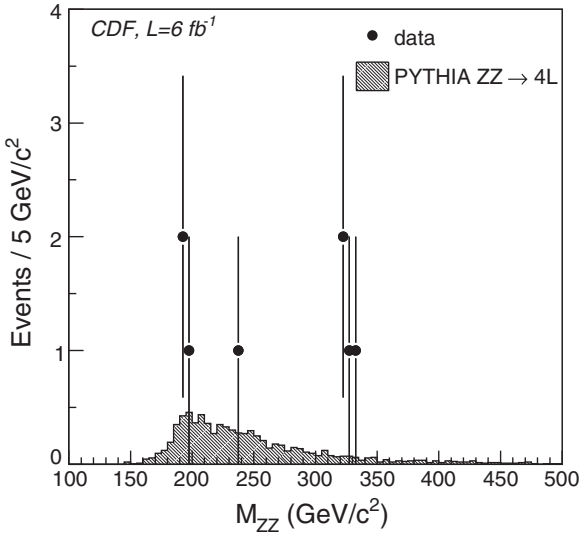

FIG. 3. M_{ZZ} for eight $ZZ \to \ell^+\ell^-\ell^+\ell^-$ candidates (PYTHIA normalized to the standard model prediction of 5.5 events).

so within detector resolution the masses of all four events are consistent with a potential new resonance.

To study the possibility that these events are due to a decay of a heavy resonance, we split the eight candidate events into low- and high-mass samples and compare the properties of the events in the two samples. The high-mass region is defined by an *a posteriori* choice $M_{ZZ} > 300\ \mathrm{GeV}/c^2$, which is $\sim 5\sigma(M_{ZZ})$ below the observed clustering of events; less than 25% of the expected standard model M_{ZZ} distribution lies above this cutoff.

The masses of the Z boson candidates for all events are shown in Fig. 4, which demonstrates that the resolution in $M_{\ell\ell}$ is consistent in the high-mass and low-mass events. Lepton identification variables are consistent with expectation for all the observed events. Most kinematic distributions for the $ZZ \to \ell^+\ell^-\ell^+\ell^-$ candidates are in agreement with standard model expectations; as one example, the p_T distributions of the 16 Z boson candidates are shown in Fig. 5.

However, for the high-mass events, the p_T distribution of the four-lepton system is rather different from the

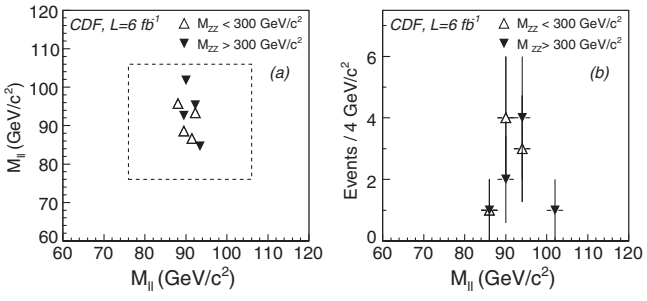

FIG. 4. Invariant masses of dilepton pairs for eight ZZ candidate events: (a) $M_{\ell\ell}(1)$ versus $M_{\ell\ell}(2)$, with selected mass region outlined; and (b) $M_{\ell\ell}$ for all Z boson candidates.

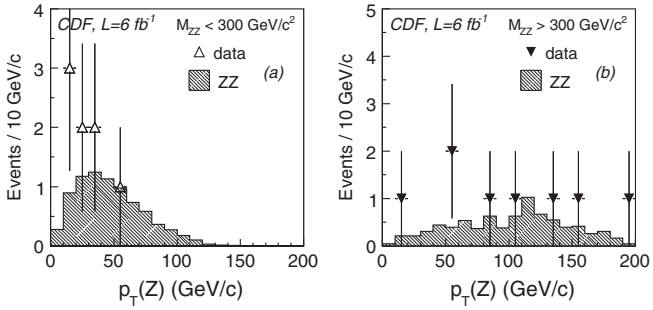

FIG. 5. p_T(Z) for Z boson candidates in (a) low-mass four-lepton candidate events and (b) high-mass events (PYTHIA prediction normalized to four events in each plot).

standard model expectation, as shown in Fig. 6. The ZZ system in the high-mass events is seen to be boosted and, as shown in Fig. 7, is recoiling against one or more jets. None of the four low-mass events has a reconstructed jet with E_T above 20 GeV.

We check whether there is any indication of misreconstruction in these events. In $ZZ \to \ell^+\ell^-\ell^+\ell^-$ events, where there is no real $\not\!\!E_T$, large measured $\not\!\!E_T$ could indicate misreconstruction. However the presence of jets broadens the detector $\not\!\!E_T$ resolution and needs to be taken into account. To this end we exploit two physics models. The first model is RS graviton production through gluon-gluon fusion (the "s-channel signal model") [7]. In order to investigate effects of the production mechanism and in the absence of a particular model that would predict the production of a boosted ZZ resonance, we take as an alternative signal model the production of a Kaluza-Klein excitation of a graviton, G^*, of $M_{G^*} = 325\ \mathrm{GeV}/c^2$ recoiling against a parton of $E_T \geq 100$ GeV (referred to as the "boosted signal model"). In both cases the HERWIG event generator is used with the full CDF detector simulation. In the four-lepton decay channel, neither of these models generates real $\not\!\!E_T$. Figure 7(b) thus demonstrates that the observed $\not\!\!E_T$ in the high-mass events is consistent with resolution effects arising from the jets.

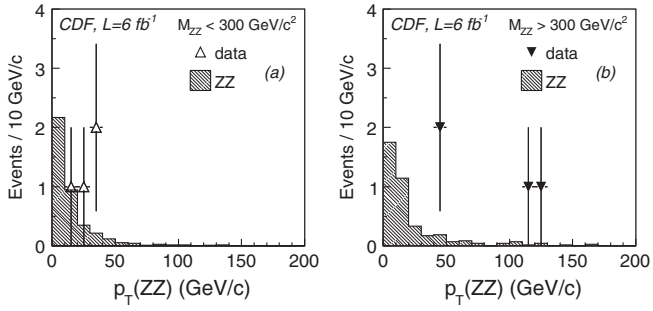

FIG. 6. $p_T(ZZ)$ for (a) low-mass four-lepton candidate events and (b) high-mass events (PYTHIA prediction normalized to four events in each plot).

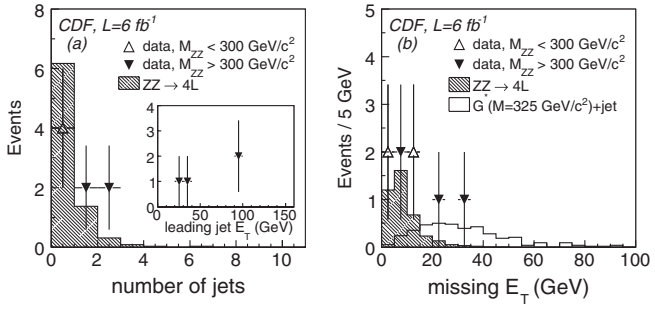

FIG. 7. (a) Number of jets and (inset) E_T of the most energetic jet; and (b) $\not\!\!E_T$ for four-lepton candidate events. $\not\!\!E_T$ distribution for $G^*(+\text{jet})$ process is normalized to 4 events.

Overall, we conclude that the observed events are well-measured and that, within the detector resolution, the kinematic parameters of the Z candidates are reconstructed correctly. The event properties are given in Table I.

To quantify consistency between the data and the standard model, we compute the probability for the observed $M_{\ell\ell\ell\ell}$ distribution to be due to a statistical fluctuation of the standard model expectation. Eight-event pseudoexperiments are drawn from the standard model M_{ZZ} distribution, and a test statistic is computed for each pseudoexperiment.

Two tests are performed. First, the Kolmogorov-Smirnov (KS) distance is taken as the test statistic, with the intention of testing for goodness-of-fit in a general way. The fraction of pseudoexperiments that has KS distance greater than that of the observed data distribution determines the computed p-value, which is found to be 0.14.

Second, a more powerful test statistic for a resonance search is used: the ratio of likelihoods of two hypotheses. The background hypothesis is provided by the standard model distribution in M_{ZZ}, M_{ZZ}^{SM}, and the signal hypothesis adds to it a resonance represented by a Gaussian peak: $f \cdot M_{ZZ}^{\mathrm{SM}} + (1-f) \cdot G(M, w)$. For a given mass M, the resonance width w is defined by the detector resolution at this mass. The resonance parameters are defined from fitting the pseudoexperiment distribution in M_{ZZ}. The likelihood ratio for the data is computed using the same procedure. The fraction of pseudoexperiments that has likelihood ratio $\mathrm{L_{SM}}/\mathrm{L_{SM+G}}$ lower than that of the observed data distribution determines the computed p-value and is found to be $(1\text{–}2) \times 10^{-3}$, where the range comes from shape differences of the PYTHIA and MC@NLO+HERWIG event generators.

In the absence of a physics model that would predict the observed $p_T(ZZ)$ distribution, we quantify consistency between the data and the standard model by computing the probability for eight events sampled from the standard model $p_T(ZZ)$ distribution to have KS distance greater than that observed in the data. The probability for the data to represent the standard model distribution is $(1\text{–}2) \times 10^{-4}$.

V. $ZZ \to \ell^+\ell^-\nu\nu$ CHANNEL

The four-lepton events observed above 300 GeV/c^2 appear somewhat anomalous. If these events were to be due to a new ZZ resonance, it would also be detectable in the other ZZ decay modes, $\ell\ell\nu\nu$ and $\ell\ell jj$. Z bosons coming from the decay of such a heavy particle would be boosted, so events with one of the Z bosons decaying into neutrinos would have large $\not\!\!E_T$. For each lepton flavor, the branching ratio to neutrinos is about twice that of charged leptons. With all three neutrino flavors included, and only one Z boson to be reconstructed, the expected event yield is around 10 times higher than in the four-lepton channel, and the sensitivity to new physics at $M_{ZZ} = 325$ GeV/c^2 is several times better than in the four-lepton channel.

Optimising sensitivity for a resonance of mass $M_{ZZ} \sim 325$ GeV/c^2, we define the search region to be $\not\!\!E_T > 100$ GeV. The standard model expectation for events with a $Z \to \ell^+\ell^-$ candidate and such high $\not\!\!E_T$ is around 25 events, as given in Table II. $Z \to e^+e^-$ and $Z \to \mu^+\mu^-$ candidates are selected according to the requirements described for the $ZZ \to \ell^+\ell^-\ell^+\ell^-$ channel. Owing to the extra acceptance, we did not reprocess the $\ell\ell + \not\!\!E_T$ data.

We validate the background model using events with a reconstructed Z boson and $\not\!\!E_T < 100$ GeV. Irreducible background contributions to a search for new physics in this channel come from standard model diboson production processes WW, WZ, and ZZ, as well as from $t\bar{t}$

TABLE I. Properties of the four-lepton candidate events, in the order in which they were recorded.

leptons	M_{Z_1}, $p_T(Z_1)$ (GeV/c^2), (GeV/c)	M_{Z_2}, $p_T(Z_2)$ (GeV/c^2), (GeV/c)	M_{ZZ} (GeV/c^2)	$p_T(ZZ)$ (GeV/c)	$\not\!\!E_T$ (GeV)	N_{jets}	Jet E_T (GeV)
$eeee$	93.3, 18.2	92.9, 17.4	196.6	35	14	0	
$\mu\mu\mu\mu$	85.9, 101.9	92.1, 54.8	321.1	47.4	8.4	1	36.7
$ee\mu\mu$	92.0, 156.0	89.9, 139.7	324.7	126.8	31	2	97.4, 40.0
$eeee$	101.3, 57.8	91.6, 13.2	334.4	44.7	9.9	1	22.7
$ee\mu\mu$	87.9, 17.7	91.8, 29.8	191.8	31	10.5	0	
$\mu\mu\mu\mu$	95.9, 197.9	92.0, 87.2	329.0	110.9	23.3	2	97.2, 24.7
$ee\mu\mu$	95.2, 36.7	89.7, 38.8	237.5	10.2	1.2	0	
$\mu\mu\mu\mu$	88.4, 51.0	89.8, 26.6	194.1	25.9	3.3	0	

TABLE II. Expected and observed event yields in the $\ell\ell + \not\!\!E_T$ channel.

Source	electron channel	muon channel
ZZ	1.8	1.3
WZ	3.6	2.8
WW	0.9	0.5
$t\bar{t}$	3.2	2.4
W + jets	0.1	0.3
Z + jets	4.0	5.1
Total standard model	13.6 ± 1.8	12.4 ± 1.6
Data	18	9
Expected s-channel signal, $M_G = 325$ GeV/c^2 and $\sigma = 1$ pb	17 ± 1	18 ± 1
Expected boosted signal, $M_G = 325$ GeV/c^2 and $\sigma = 1$ pb	20 ± 1	17 ± 1

production. Other non-negligible background contributions come from Z + jets events that have large $\not\!\!E_T$ due to jet mismeasurement; from W + jets events where one of the jets is misreconstructed as a lepton and forms a Z boson candidate with the charged lepton from the decay of the W boson; and, in the $ee + \not\!\!E_T$ channel, from $W\gamma$ production with the photon misreconstructed as an electron.

Irreducible backgrounds are estimated using the PYTHIA generator and the full CDF detector simulation, normalized to NLO cross sections [25]. The Z + jets contribution is also estimated using PYTHIA simulation and is normalized using a subset of the $\not\!\!E_T < 100$ GeV data. As Z + jets events have high $\not\!\!E_T$ only through misreconstruction, the normalization is carried out on events having $50 < \not\!\!E_T < 100$ GeV that also have a small angle $\Delta\phi_{\rm min}$ between the $\not\!\!E_T$ and the closest jet, or lepton, reconstructed in the event: $|\Delta\phi_{\rm min}| < 0.5$. The $|\Delta\phi_{\rm min}|$ distribution is shown in Fig. 8(a). It is verified that this procedure is not sensitive to the $\not\!\!E_T$ range used.

The background contribution from the W + jets process is estimated from a data sample where events contain an identified lepton and an additional jet. These events are weighted by jet-to-lepton misidentification rates as described in Section IV to estimate the total yield. Owing to differences in jet-to-lepton fake rates between electrons and muons, the W + jets contribution is found to be negligible in the $\mu\mu + \not\!\!E_T$ channel, but non-negligible in the $ee + \not\!\!E_T$ channel.

Photon conversions are the primary source of jets being misidentified as electrons, and so W + jets events result in approximately equal numbers of same-charged and oppositely-charged candidate events. The estimate is therefore validated against the sample of events that have two lepton candidates of the same charge and $50 < \not\!\!E_T < 100$ GeV. Figure 8(b) shows that this selection is dominated by W + jets. The estimate is also cross-checked by applying the same misidentification rates to $W^{\pm} \to e^{\pm}\nu$ simulation normalized to the NLO production cross section. The two methods give results consistent within 10%.

The overall modeling of the sample composition is demonstrated by the $\not\!\!E_T$ spectrum shown in Fig. 9. The largest relative uncertainty in this channel comes from the Z + jets normalization, and is 10% and 13% in the electron and muon channels, respectively. Other uncertainties come from lepton identification (2%), acceptance ($< 1\%$), cross sections of diboson and top-quark production (5% and 10%), and the fake lepton background (20%). The total background uncertainty is 13%.

To search for a high-mass resonance we examine events with $\not\!\!E_T > 100$ GeV. Event yields are given in Table II. In electron and muon channels combined we expect 26 events from standard model processes, and observe 27. Four four-lepton events around $M_{ZZ} = 325$ GeV/c^2 coming from the decay of a new state would imply a production cross section times branching ratio to ZZ close to 1 pb, and for that cross section, the s-channel G^* signal model predicts around 35 additional events.

As the second Z boson in this channel decays into neutrinos, the invariant mass of the Z pair cannot be fully

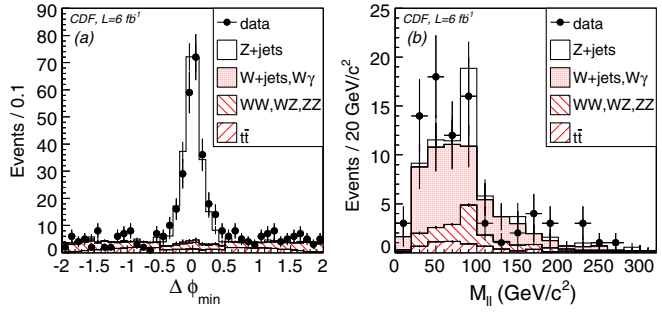

FIG. 8 (color online). (a) $\Delta\phi_{\rm min}$ as used for Z + jets normalization, and (b) $M_{\ell\ell}$ for same-sign dielectron pairs with large $\not\!\!E_T$ used to validate the W + jets background estimation.

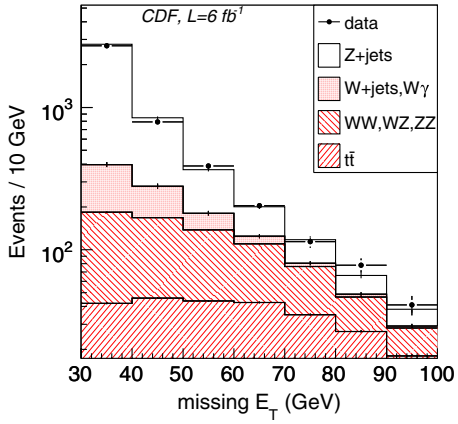

FIG. 9 (color online). $\not\!\!E_T$ distribution for events with opposite sign lepton pairs ($ee + \mu\mu$). The contribution of Z + jets events is normalized in the region $50 < \not\!\!E_T < 100$ GeV using events with low $|\Delta\phi_{\rm min}|$.

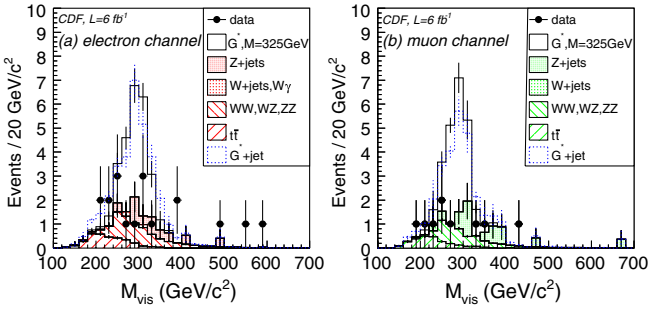

FIG. 10 (color online). M_{ZZ}^{vis} for (a) the electron and (b) muon channels. The expected contribution from a graviton of $M_{G^*} = 325\ \mathrm{GeV}/c^2$ and cross section times branching ratio to ZZ of 1 pb is shown together with the expected contribution of boosted G^*, produced in association with a jet. The high values of M_{ZZ}^{vis} of three events in the electron channel are understood as originating from fluctuations of the jet energy losses in events with high jet activity.

reconstructed. The closest approximation is the "visible mass" M_{ZZ}^{vis}, defined as the invariant mass of the sum of the two charged lepton four-momenta and the four-vector representing the $\not\!\!E_T$, $(\not\!\!E_x, \not\!\!E_y, 0, |\not\!\!E_T|)$. Figure 10 shows the M_{ZZ}^{vis} distribution in the signal region, $\not\!\!E_T > 100$ GeV, with the expected distribution for an RS graviton of mass $M_{G*} = 325\ \mathrm{GeV}/c^2$ and cross section times branching ratio of 1 pb overlaid. In this channel we find little difference in expected distributions or yields between the two signal models, confirming that the analysis is not strongly dependent on the detail of the models. Neither the event counts of Table II, nor the distributions of Fig. 10, show any evidence for a resonance decaying into ZZ.

VI. $ZZ \to \ell^+\ell^- jj$ CHANNEL

The decay of a heavy particle into two Z bosons where one of the Z bosons decays into charged leptons and the other to jets has the advantage of being fully reconstructible, and the event yield in the $\ell\ell jj$ channel is expected to be around 20 times higher than in the four-lepton channel.

$Z \to e^+e^-$ and $Z \to \mu^+\mu^-$ candidates are selected according to the requirements described for the $ZZ \to \ell^+\ell^-\ell^+\ell^-$ channel, and a further requirement is made of at least two reconstructed jets having corrected $E_T > 25$ GeV. To reconstruct the second Z boson candidate, all pairs of jets are considered and if there is a pair with invariant mass between 70 and 110 GeV/c^2 it is accepted. This inclusive selection, with the additional requirement of the invariant mass of the two Z candidates being less than 300 GeV/c^2, defines a control region.

This channel is dominated by Z + jets events. Other standard model sources, small compared with Z + jets, are WZ and ZZ production, and $t\bar{t}$ production. The contributions from WW and W + jets events are negligible.

Diboson and $t\bar{t}$ event yields are estimated using PYTHIA Monte Carlo normalized to NLO cross sections. Z + jets events are modeled using the generator ALPGEN [28] interfaced with PYTHIA for parton showering and hadronization, and the normalization of the Z + jets contribution is obtained by fitting to the total data yield in the control region. The detector acceptance is different for $Z \to e^+e^-$ and $Z \to \mu^+\mu^-$ and so the Z + jets normalization factors for the two channels are not expected to be identical. The difference between them is indicative of the systematic uncertainty, leading to a total background uncertainty of 10%. The jet multiplicity distributions in the control region, shown in Fig. 11, demonstrate the good background modeling.

In the $\ell\ell jj$ final state we improve the resolution in the reconstructed M_{ZZ} by varying jet four-momenta within their uncertainties and constraining the reconstructed invariant masses M_{jj} to the mass of the Z boson, M_Z. The resolution in M_Z for $Z \to jj$ is 15 GeV/c^2, which is much larger than the intrinsic width of the Z boson. In the $\ell\ell jj$ channel the constraining procedure therefore improves the mass resolution of the ZZ candidates, to 12 GeV/c^2 for $M_{G^*} = 325\ \mathrm{GeV}/c^2$. As the detector resolution for M_Z in $Z \to \ell^+\ell^-$ is comparable with the intrinsic width of the Z boson, applying the mass-constraining procedure to the leptons has very little effect on the M_{ZZ} resolution and is used only as a cross-check. Throughout this paper $M_{\ell\ell jj}$ refers to the constrained four-object invariant mass.

To search for a high-mass resonance we examine the complete $M_{\ell\ell jj}$ spectrum. Z bosons coming from the decay of a heavy particle would be boosted, and optimization studies result in requiring the most energetic jet in the $Z \to jj$ candidate to have $E_T > 50$ GeV and the p_T of either the $Z \to jj$ or $Z \to \ell^+\ell^-$ candidate to be greater than 75 GeV/c. Observed event yields are given in Table III and are consistent with standard model expectations. A resonance of $M_{G^*} = 325\ \mathrm{GeV}/c^2$ and cross section times branching ratio to ZZ of 1 pb would be expected to yield around 30 events in the muon channel and 40 events in the electron channel, and as the $ZZ \to \ell^+\ell^- jj$ final state is

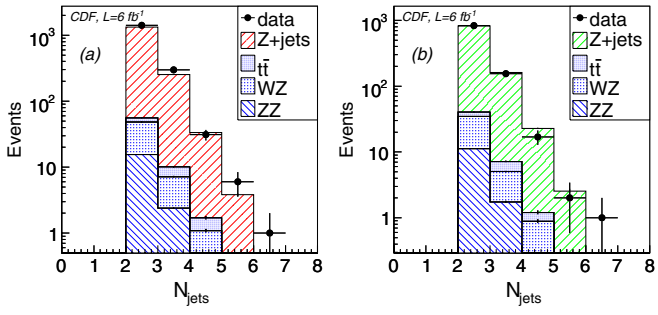

FIG. 11 (color online). Number of jets in (a) $Z \to e^+e^-$ + ≥ 2 jets and (b) $Z \to \mu^+\mu^-$ ≥ 2 jets events in the control region $M_{\ell\ell jj} < 300\ \mathrm{GeV}/c^2$.

TABLE III. Expected and observed event yields in the $\ell\ell jj$ channel.

Source	electron channel	muon channel
ZZ	6	5
WZ	17	12
$t\bar{t}$	7	5
Z + jets	395	244
Total standard model	424 ± 40	266 ± 24
Data	392	253
Expected signal, $M_G = 325$ GeV/c^2 and $\sigma = 1$ pb	41 ± 1	32 ± 1

fully reconstructed, they would appear as a narrow peak in $M_{\ell\ell jj}$. Figure 12 shows the $M_{\ell\ell jj}$ distribution for the $eejj$ and $\mu\mu jj$ channels, with the standard model and additional ZZ resonance model predictions.

Studies of systematic effects resulting from the generator Q^2 scale choice and from the jet energy scale uncertainty show that they do not affect the expected shapes of the $M_{\ell\ell jj}$ distributions. We investigate potential effects of the production mechanism using the alternative boosted G^* signal model. Motivated by the anomalous $p_T(ZZ)$ distribution shown by the events in the four-lepton channel, the signal selection is modified to require $p_T(\ell\ell jj) > 40$ GeV/c, which further suppresses standard model background, The resulting $M_{\ell\ell jj}$ distribution and boosted G^* prediction is shown in Fig. 13. As with the $\ell\ell + \not\!\!E_T$ channel there are no statistically significant differences from the standard model expectation.

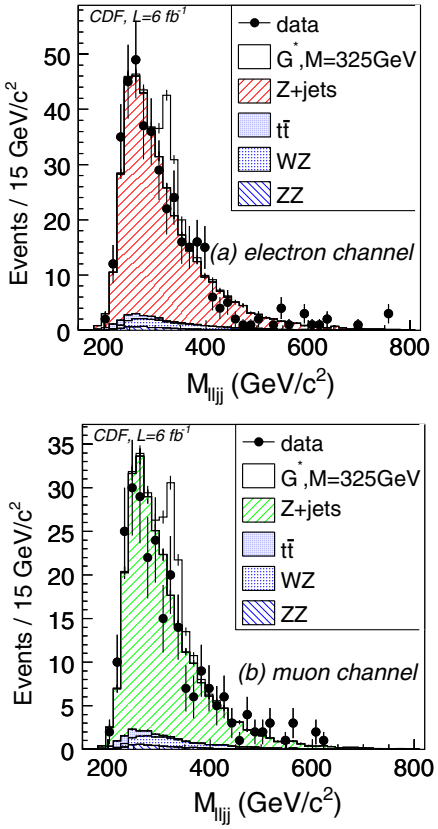

FIG. 12 (color online). $M_{\ell\ell jj}$ for the (a) electron and (b) muon channels, showing the expected contribution from a graviton of $M_{G^*} = 325$ GeV/c^2 and cross section times branching ratio to ZZ of 1 pb.

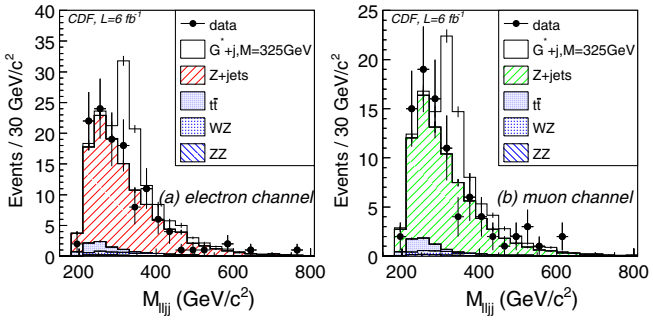

FIG. 13 (color online). $M_{\ell\ell jj}$ for the (a) electron and (b) muon channels for $p_T(ZZ) > 40$ GeV/c, showing the expected contribution from a boosted graviton of $M_{G^*} = 325$ GeV/c^2 and cross section times branching ratio to ZZ of 1 pb.

VII. LIMITS

To quantify results of the search we compute expected and observed limits on the production cross section times branching ratio $\sigma(p\bar{p} \to G^* \to ZZ)$.

The expected sensitivity is determined with a Bayesian technique [29], using CL S likelihood test statistics [30] to perform a binned maximum-likelihood fit over the M_{ZZ}, M_{ZZ}^{vis}, and $M_{\ell\ell jj}$ distributions in the four-lepton, $\ell\ell + \not\!\!E_T$, and $\ell\ell jj$ channels, respectively. The background hypothesis is provided by the standard model expectation as described in Sections IV, V, and VI. Background-only pseudo-experiments are drawn from Monte Carlo simulation. In the fit, the background templates can fluctuate within their uncertainties. A test statistic is formed from

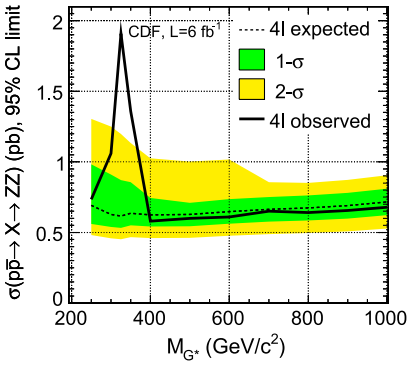

FIG. 14 (color online). Expected and observed 95% CL limits on $\sigma(p\bar{p} \to G^* \to ZZ)$ from the four-lepton channel; the four events with $M_{ZZ} = 327$ GeV/c^2 result in a deviation from the expected limit.

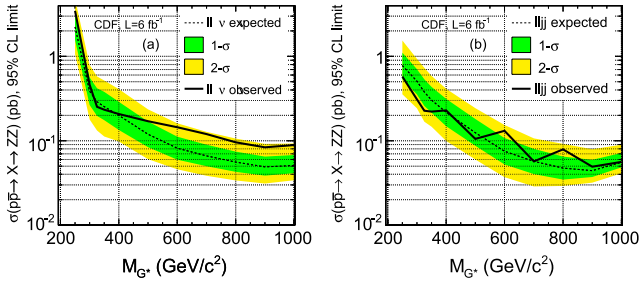

FIG. 15 (color online). Expected and observed 95% CL limits on $\sigma(p\bar{p} \to G^* \to ZZ)$ from (a) the $ZZ \to \ell^+\ell^-\nu\nu$ channel, and (b) the $ZZ \to \ell^+\ell^- jj$ channel.

the difference in the likelihoods between the background-only model and the signal-plus-background model at the best fit values for the pseudo-experiment. From this, expected 95% credibility level (CL) upper limits on cross section times branching ratio are extracted.

Figure 14 shows expected and observed limits in the four-lepton channel for G^* masses between 250 and 1000 GeV$/c^2$. At $M_{G^*} = 325$ GeV$/c^2$ the expected sensitivity is around 0.7 pb, and the four events with masses clustered around that value result in an observed limit of 1.9 pb.

Although the backgrounds in the $\ell\ell + \not\!\!E_T$ channel are higher than in the four-lepton channel, this channel provides better sensitivity. Figure 15(a) shows the expected and observed cross section limits for $\ell\ell + \not\!\!E_T$, and there are no large differences from standard model expectations. For $M_{G^*} = 325$ GeV$/c^2$ the expected 95% CL upper cross section limit on the s-channel signal model is 0.29 pb, and the observed limit is 0.25 pb. For the boosted G^* signal model the 95% CL expected and observed limits are both 0.30 pb. This is a change of less than 10% from the s-channel model, demonstrating that the analysis sensitivity is not strongly dependent on the detail of the production model.

Figure 15(b) shows the expected and observed cross section limits for the $\ell\ell jj$ channel. Here the expected 95% CL upper cross section limit is 0.38 pb for $M_{G^*} = 325$ GeV$/c^2$, and the observed limit is 0.23 pb. With the selection tuned for a boosted signal model, $p_T(\ell\ell jj) > 40$ GeV$/c$, the sensitivity is improved slightly compared to the s-channel signal model. The expected limit is 0.27 pb and the observed limit is 0.26 pb, showing that also in this channel the analysis sensitivity is not strongly dependent on the detail of the signal model.

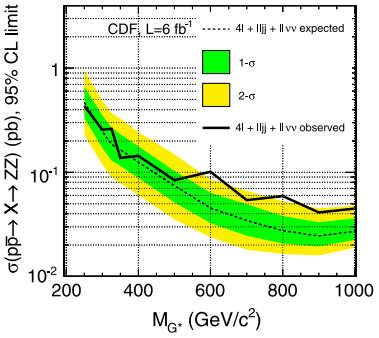

FIG. 16 (color online). Expected and observed 95% CL limits on $\sigma(p\bar{p} \to G^* \to ZZ)$ from all channels combined.

Combining all three channels results in the most sensitivity. Expected and observed limits are consistent with each other, as shown in Fig. 16. For $M_{G^*} = 325$ GeV$/c^2$ the sensitivity is dominated by the $\ell\ell + \not\!\!E_T$ channel. For an s-channel resonance, the 95% CL upper cross section limit is expected to be 0.19 pb and is observed to be 0.26 pb. For a boosted resonance of $M_{G^*} = 325$ GeV$/c^2$ the expected limit is 0.17 pb and the observed limit is 0.28 pb.

VIII. CONCLUSIONS

We have searched for heavy resonances decaying into Z boson pairs using the final states consisting of four leptons, two leptons and $\not\!\!E_T$, and two leptons plus jets. In the channel with the smallest background, the four-lepton channel, we have observed eight candidate events. Four events with high values of ZZ mass are close in mass, and two of those have unusually high $p_T(ZZ)$.

However, more sensitive searches in the $\ell\ell + \not\!\!E_T$ and $\ell\ell jj$ final states show no indication of a new heavy particle decaying to two Z bosons, suggesting that the events observed around 325 GeV$/c^2$ in the four-lepton channel result from standard model processes. Combining all three channels we set upper limits on the cross section times branching ratio $\sigma(p\bar{p} \to G^* \to ZZ)$ that vary between 0.26 pb and 0.045 pb in the mass range $300 < M_{G^*} < 1000$ GeV$/c^2$, and the limits do not depend strongly on the production model.

ACKNOWLEDGMENTS

We thank the Fermilab staff and the technical staffs of the participating institutions for their vital contributions. This work was supported by the U.S. Department of Energy and National Science Foundation; the Italian Istituto Nazionale di Fisica Nucleare; the Ministry of Education, Culture, Sports, Science and Technology of Japan; the Natural Sciences and Engineering Research Council of Canada; the National Science Council of the Republic of China; the Swiss National Science Foundation; the A. P. Sloan Foundation; the Bundesministerium für Bildung und Forschung, Germany; the Korean World Class University Program, the National Research Foundation of Korea; the Science and Technology Facilities Council and the Royal Society, UK; the Russian Foundation for Basic Research; the Ministerio de Ciencia e Innovación, and Programa Consolider-Ingenio 2010, Spain; the Slovak R&D Agency; the Academy of Finland; and the Australian Research Council (ARC).

[1] D. de Florian and M. Grazzini, Phys. Lett. B **674**, 291 (2009); C. Anastasiou, R. Boughezal, and F. Petriello, J. High Energy Phys. 04 (2009) 003; A. Djouadi, J. Kalinowski, and M. Spira, Comput. Phys. Commun. **108C**, 56 (1998).

[2] M. Kober, B. Koch, and M. Bleicher, Phys. Rev. D **76**, 125001 (2007).

[3] L. Randall and R. Sundrum, Phys. Rev. Lett. **83**, 3370 (1999).

[4] The coupling must be large enough to be consistent with the apparent weakness of gravity but small enough to prevent the theory from becoming nonperturbative. A natural choice is $k/M_{\mathrm{Pl}} = 0.1$, where k is a curvature parameter and M_{Pl} is the Planck scale.

[5] T. Aaltonen *et al.* (CDF Collaboration), Phys. Rev. Lett. **107**, 051801 (2011); V. Abazov *et al.* (D0 Collaboration), Phys. Lett. B **695**, 88 (2011); G. Aad *et al.* (ATLAS Collaboration), Phys. Lett. B **700**, 163 (2011); S. Chatrchyan *et al.* (CMS Collaboration), J. High Energy Phys. 05 (2011) 093.

[6] K. Agashe, H. Davoudiasl, G. Perez, and A. Soni, Phys. Rev. D **76**, 036006 (2007).

[7] L. Fitzpatrick, J. Kaplan, L. Randall, and L. Wang, J. High Energy Phys. 09 (2007) 013.

[8] T. Aaltonen *et al.* (CDF Collaboration), Phys. Rev. D **83**, 112008 (2011).

[9] R. Blair *et al.* (CDF Collaboration), Report No. FERMILAB-Pub-96/390-E.

[10] A. Sill *et al.*, Nucl. Instrum. Methods Phys. Res., Sect. A **447**, 1 (2000).

[11] T. Affolder *et al.*, Nucl. Instrum. Methods Phys. Res., Sect. A **526**, 249 (2004).

[12] L. Balka *et al.*, Nucl. Instrum. Methods Phys. Res., Sect. A **267**, 272 (1988).

[13] S. Bertolucci *et al.*, Nucl. Instrum. Methods Phys. Res., Sect. A **267**, 301 (1988).

[14] G. Ascoli *et al.*, Nucl. Instrum. Methods Phys. Res., Sect. A **268**, 33 (1988).

[15] D. Acosta *et al.*, Nucl. Instrum. Methods Phys. Res., Sect. A **494**, 57 (2002).

[16] A. Abulencia *et al.* (CDF Collaboration), J. Phys. G **34**, 2457 (2007).

[17] F. Abe *et al.* (CDF Collaboration), Phys. Rev. D **44**, 29 (1991).

[18] F. Abe *et al.* (CDF Collaboration), Phys. Rev. D **45**, 1448 (1992).

[19] A. Bhatti *et al.*, Nucl. Instrum. Methods Phys. Res., Sect. A **566**, 375 (2006).

[20] T. Sjöstrand *et al.*, Comput. Phys. Commun. **135**, 238 (2001).

[21] E. Gerchtein and M. Paulini, Report No. CHEP-2003-TUMT005.

[22] S. Frixione and B. R. Webber, J. High Energy Phys. 06 (2002) 029.

[23] G. Corcella *et al.*, J. High Energy Phys. 01 (2001) 010.

[24] K. Nakamura *et al.* (Particle Data Group), J. Phys. G **37**, 075021 (2010).

[25] J. M. Campbell and R. K. Ellis, Phys. Rev. D **60**, 113006 (1999); N. Kidonakis and R. Vogt, Phys. Rev. D **78**, 074005 (2008).

[26] G. J. Feldman and R. D. Cousins, Phys. Rev. D **57**, 3873 (1998).

[27] T. Aaltonen *et al.* (CDF Collaboration) arXiv:1112.2978.

[28] M. L. Mangano *et al.*, J. High Energy Phys. 07 (2003) 001.

[29] J. Heinrich and L. Lyons, Annu. Rev. Nucl. Part. Sci. **57**, 145 (2007).

[30] T. Junk, Nucl. Instrum. Methods Phys. Res., Sect. A **434**, 435 (1999).